Spectrochimica Acta Part B 70 (2012) 45–50

Contents lists available at SciVerse ScienceDirect

Spectrochimica Acta Part B

journal homepage: www.elsevier.com/locate/sab

Quantitative laser-induced breakdown spectroscopy of potassium for in-situ geochronology on Mars

Christopher B. Stipe [a,*], Edward Guevara [a], Jonathan Brown [a], George R. Rossman [b]

[a] Department of Mechanical Engineering, Seattle University, Seattle, WA 98122, USA
[b] Division of Geological and Planetary Sciences, California Institute of Technology, Pasadena, CA 91125, USA

ARTICLE INFO

Article history:
Received 30 December 2011
Accepted 24 April 2012
Available online 3 May 2012

Keywords:
Laser-induced breakdown spectroscopy
Geochronology
K–Ar dating
Potassium
Mars

ABSTRACT

Laser-induced breakdown spectroscopy is explored for the development of an in-situ K–Ar geochronology instrument for Mars. Potassium concentrations in standard basaltic glasses and equivalent rock samples in their natural form are quantified using the potassium doublet at 766.49 and 769.90 nm. Measurement precision varies from 0.5 to 5.5 (% RSD) over the 3.63% to 0.025% potassium by weight for the standard samples, and little additional precision is achieved above 20 laser shots at 5 locations. For the glass standards, the quantification limits are 920 and 66 ppm for non-weighted and weighted calibration methods, respectively. For the basaltic rocks, the quantification limits are 2650 and 328 ppm for the non-weighted and weighted calibration methods, respectively. The heterogeneity of the rock samples leads to larger variations in potassium signal; however, normalizing the potassium peak by base area at 25 locations on the rock improved calibration accuracy. Including only errors in LIBS measurements, estimated age errors for the glasses range from approximately ±30 Ma for 3000 Ma samples to ±2 Ma for 100 Ma samples. For the basaltic rocks, the age errors are approximately ±120 Ma for 3000 Ma samples and ±8 Ma for 100 Ma samples.

1. Introduction

The study of Martian geological history is hindered by the absence of direct absolute age characterization of surface materials of known geographical location. While the relative chronology of Martian surfaces has been accomplished through stratigraphic studies [1], a direct measure of absolute age has not yet been achieved. Instead, indirect estimates of absolute age are extrapolated from lunar cratering densities correlated to age-dated return samples from Apollo and Luna missions [2,3]. Known sources of errors for this approach include secondary craters formed by impact ejecta and crater resurfacing by erosion and deposition [4,5]. Hartmann estimates a factor of 2–4 uncertainty in age dating when extrapolating from lunar to Martian cratering densities [5]. Additionally, it has been shown that differences in crater counting techniques lead to age determinations that vary between 5% and 20% [6]. Precisely aged Martian meteorites shed light on the planet's volcanic activity and the existence of old geological material (ALH84001) [7]; yet, they cannot be used to correlate cratering densities because the place of origin of these meteorites is unknown.

Both sample return and in-situ geochronology measurements are being explored to solve this problem, each with associated advantages and disadvantages. While returned samples provide the best option for obtaining accurate age measurements, as the samples will be available for measure by an array of techniques in multiple laboratories, the engineering challenges associate with a robotic launch from the surface of Mars are substantial. Maybe more importantly, the returned sample approach does not allow for iteration between sample selection and corresponding age measurements; thus, if the correct compositional or age range of rocks is not collected to accurately correlate crater densities, a costly second mission would be required. In-situ measurements would allow for this experimental iteration, at the cost of precision and accuracy. The best approach may be to include an in-situ technique in a sample return mission as a sample selection tool. Potassium–Argon dating shows promise as an in-situ technique suitable for Mars [8]. As envisioned, a possible system will consist of two instruments: (1) a heating chamber or laser heating system with a mass spectrometer to measure outgassed argon and (2) a laser-induced breakdown spectroscopy (LIBS) instrument to measure potassium. In our paper, we evaluate LIBS for quantifying potassium abundance.

LIBS is a spectroscopic method where atomic emission from a laser generated plasma is collected to identify and quantify elemental abundances [9]. The Mars Science Laboratory rover, launched in the fall of 2011, includes a LIBS instrument as part of the ChemCAM suite [10,11]. The performance of LIBS for elemental quantification of geological materials has been extensively studied under simulated Martian environmental conditions. Knight et al. observed signal enhancements of 3–4 times under Martian atmospheric pressure and composition compared to the atmospheric conditions on earth [12]. This signal enhancement is due to the reduced pressure which improves laser ablation of material from the surface by reducing attenuation of the

* Corresponding author at: 901 12th Avenue, Seattle, WA 98122. Tel.: +1 206 296 6941; fax: +1 206 296 2209.
E-mail address: stipec@seattleu.edu (C.B. Stipe).

0584-8547/$ – see front matter © 2012 Elsevier B.V. All rights reserved.
doi:10.1016/j.sab.2012.04.010

laser energy by plasma shielding [9]. Clegg et al. have explored multivariate spectral analysis methods to reduce matrix effects [11], and accuracies on the order of ±10% have been achieved for most elements [13]. Dell'Aglio et al. performed LIBS measurements on six Martian, lunar, and other meteorites [14] to identify and quantify elements for geological classification. For major elements with weight concentrations above 6%, prediction errors ranged from approximately 0.5% to 15%. For minor elements, prediction errors were as high as 60%. Thompson et al. analyzed two Martian basaltic shergottite meteorites (DaG 476 and Zagami) by LIBS and achieved oxide weight percent differences from literature values from 4% to 79% [15]. Again, higher concentrated elements were better predicted than elements of lower concentration.

Colao et al. studied the feasibility of LIBS as an in-situ instrument by measuring NIST standard reference soils and Martian rock analogues [16]. Quantifying potassium in NIST standard reference soils pressed into pellets, they achieved accuracies of prediction between 12% and 30%. The predicted concentrations were consistently lower than known concentrations, which the authors attribute to signal saturation and self-absorption. Measuring potassium in silicate materials, LIBS predicted concentrations were approximately 40% lower than those measured by EDX. In their study, eleven elements were measured simultaneously, making it difficult to optimize experimental parameters for any one specific element. In our study, we focus solely on measuring potassium by LIBS in an effort to develop an in-situ K–Ar geochronology instrument.

Currently, only a small amount of preliminary work exists in the literature on the development of K–Ar dating using LIBS to quantify potassium. Swindle et al. [17] provide a LIBS calibration curve for samples containing up to about 6% potassium by weight. Solé [18] also proposes the technique, showing a representative spectrum of potassium by LIBS.

The three naturally occurring potassium isotopes of ^{39}K (93.2851%), ^{40}K (0.0117%), and ^{41}K (6.7302%) are simultaneously detected by LIBS due to the physical broadening of the emission peaks and the limited resolving power of common LIBS spectrometers. Potassium-40 is radiogenic and decays with a half-life of 1.248×10^{9} years, while ^{39}K and ^{41}K are stable. The equation for determining time since crystallization in terms of the initial and final ^{40}K abundances is:

$$t = \frac{t_{1/2}}{\ln(2)} \ln \frac{\left[^{40}\mathrm{K}\right]_i}{\left[^{40}\mathrm{K}\right]_f} \quad (1)$$

where t is the elapsed time since crystallization, $t_{1/2}$ is the half-life of ^{40}K, $[^{40}\mathrm{K}]_i$ is the original ^{40}K abundance, and $[^{40}\mathrm{K}]_f$ is the final ^{40}K abundance. This standard form of the elapsed-time equation is modified in two ways. First, a substitution is made because the original concentration of ^{40}K cannot be directly measured. Accounting for the 10.48% of ^{40}K decay events that result in ^{40}Ar, the substitution becomes:

$$\left[^{40}\mathrm{Ar}\right]_f = 0.1048\cdot\left(\left[^{40}\mathrm{K}\right]_i - \left[^{40}\mathrm{K}\right]_f\right) \quad (2)$$

Second, Eq. (1) must reflect that all isotopes of potassium will be measured simultaneously. Assuming that the concentrations of the stable isotopes do not change with time and that the change in the ^{40}K is small (near the detection limit of LIBS) compared to the total LIBS potassium signal, the final elapsed-time equation becomes:

$$t = \frac{t_{1/2}}{\ln(2)} \ln\left(\frac{\left[^{40}\mathrm{Ar}\right]_f}{0.1048\cdot1.17\cdot10^{-4}\left[^{39}\mathrm{K}+^{40}\mathrm{K}+^{41}\mathrm{K}\right]_f}+1\right) \quad (3)$$

where $[^{40}\mathrm{Ar}]_f$ is the final abundance of ^{40}Ar and $[^{39}\mathrm{K}+^{40}\mathrm{K}+^{41}\mathrm{K}]_f$ is the final potassium abundances measured by LIBS. Argon-40 will be measured by sample heating and mass spectrometry. Technical challenges with correcting for excess ^{40}Ar will be addressed in a later publication describing the mass spectrometer measurements.

In this study, we investigate the efficacy of LIBS for quantifying potassium in standard basaltic glass and natural basaltic rock samples. Experimental parameters are explored to understand their influence on LIBS potassium signal. Potassium calibration curves are generated to determine measurement accuracy and resulting errors in age quantification.

2. Experimental

Laser-induced breakdown spectroscopy measurements were performed with a Photon Machines Insight™ LIBS system. A representative schematic of the experimental apparatus was published previously [19]. The laser-induced plasma was generated by a frequency quadrupled Nd:YAG laser emitting 266 nm, 7 ns laser pulses with a beam diameter of 5 mm, a maximum energy of 35 mJ, and a shot-to-shot energy stability of ±2%. The 266 nm light was better absorbed by the basaltic glass samples than the fundamental and doubled laser frequencies. After exiting the laser, the beam is expanded, collimated, and then focused onto the sample surface using a 5× microscope objective. The laser spot size at the sample surface is controlled by varying the distance between the beam expander and collimator. Imaging of the sample surface with a video camera ensured a constant lens-to-sample distance for samples of different thicknesses. Optical emission was collected through a 400 μm diameter fiber optic cable aimed 50 degrees from the vertical axis. The collected light entered a 50×50 μm slit into an echelle spectrometer (Catalina Scientific model SE 200) with a resolving power of $\lambda/\Delta\lambda \sim 1700$. The dispersed light was imaged by an iCCD camera (Andor iStar model DH734i). Chip read-out time limited the acquisition rate to 1 Hz.

3. Samples

Five USGS standard basaltic glass samples (BIR-1G, BHVO-2G, BCR-2G, NKT-1G, and TB-1G) were used in this study (see Table 1). Of these five samples, four of the rocks in their natural form were also acquired and measured (BIR-1, BHVO-2, BCR-2, NKT-1), and the potassium concentration of these samples were determined by whole rock analysis (Florin Analytical Services, Reno, NV, USA). To conserve the more expensive standard basaltic glasses, LIBS signal optimization studies were performed on a sample of obsidian (Glass Buttes, OR), containing approximately 3% potassium by weight.

4. Results and discussion

Experimental parameters including spectrometer delay, laser pulse energy, and laser spot size strongly influence the potassium signal. The potassium doublet, shown in Fig. 1, emits fluorescence at 766.49 nm ($^2P_{3/2}\rightarrow{}^2S_{1/2}$) and 769.90 nm ($^2P_{1/2}\rightarrow{}^2S_{1/2}$). The upper and lower energy levels for these transitions are given in Table 2. Both transitions

Table 1
Elemental compositions of basaltic glass standards and equivalent basaltic rocks. Concentrations are in weight %.

Sample	Basaltic glass standards					Basaltic rocks			
	BIR-1G	BHVO-2G	NKT-1G	BCR-2G	TB-1G	BIR-1	BHVO-2	NKT-1	BCR-2
Al	8.20	7.16	5.39	7.14	8.83	8.35	7.30	5.63	7.38
Ca	9.51	8.17	9.44	5.09	4.91	9.12	7.27	9.03	4.96
Fe	7.90	8.63	9.32	9.65	6.33	8.22	9.38	9.24	10.01
K	**0.025**	**0.43**	**1.06**	**1.49**	**3.63**	**0.03**	**0.51**	**1.28**	**1.64**
Mg	5.85	4.36	8.64	2.16	2.20	6.18	4.26	7.84	2.19
Na	1.35	1.64	2.58	2.34	2.37	1.34	1.72	2.60	2.33
P	0.01	0.12	0.42	0.15	0.26	0.01	0.15	0.45	0.11
Si	22.39	23.30	18.08	25.30	25.34	21.63	23.01	17.82	24.46
Ti	0.58	1.63	2.37	1.35	0.51	0.55	1.57	2.38	1.33

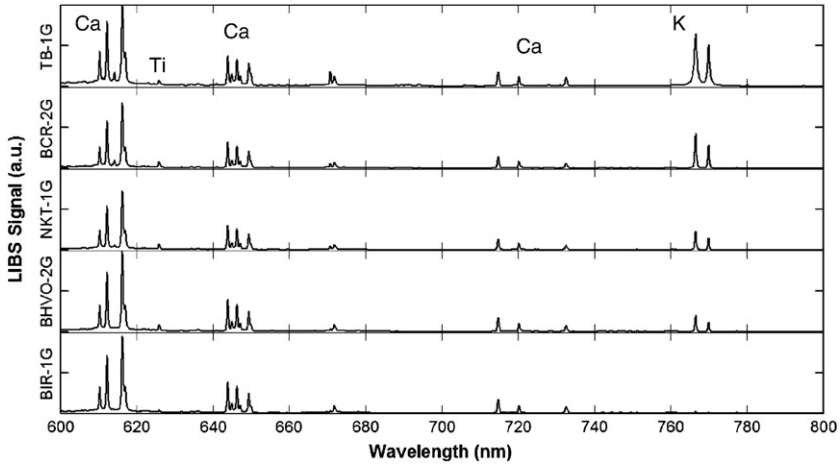

Fig. 1. Representative spectra for five USGS standard basaltic glasses. Spectra were generated with 35 mJ pulses, 500 μm laser spots, and a delay and gate of 1.5 μs and 3 μs, respectively.

terminate in the ground state. For all optimization measurements, the potassium signal was obtained by area integration of both peaks with baseline subtraction.

4.1. Spectrometer delay

The acquisition of light by the echelle spectrometer and iCCD camera is delayed in time from the laser emission. Delaying the initiation of the acquisition protects the camera from saturation by intense scattered laser light and allows the continuum plasma emission to decay, improving signal to noise [20]. Fig. 2 shows the relationship between potassium signal and spectrometer delay using a 1 μs gate, 500 μm laser spot, and 35 mJ pulse energy. The signals are averages of 50 shots in the same location acquired after 5 cleaning shots. Error bars are one standard deviation over the 50 shots. The upper energy levels for the potassium doublet are 1.617 and 1.610 eV for the 766.45 and 769.90 nm peaks, respectively. For both peaks, emission occurs to the ground state (0 eV) and emission is strongest early in the plasma lifetime. A delay time of 1.5 μs was chosen for all measurements described below.

4.2. Laser pulse energy

The potassium signal dependence on laser pulse energy is shown in Fig. 3. Pulse energy was varied from 7 mJ to 35 mJ at with a laser spot size of 500 μm, corresponding to power densities from 0.5 to 2.5 GW/cm^2, respectively. Below 0.5 GW/cm^2, no plasma formation or potassium signal was observed. The highest potassium signal occurred at 35 mJ, which was the maximum energy achievable with the laser. The maximum signal likely occurs above 35 mJ; however, it can be seen that the rise in potassium signal begins to fall off at 30 mJ, caused by plasma shielding of the laser [9].

4.3. Laser spot size

Fig. 4 shows the potassium signal dependence on laser spot size at a pulse energy of 35 mJ. Major fracturing of the obsidian sample, and erratic LIBS signals, occurred at and below a spot size of 150 μm (~28 GW/cm^2). From 200 to 500 μm, the potassium signal increases with spot size, while the signal decreases above 500 μm.

Table 2
Spectral location and electronic energy levels of atomic emission for potassium.

Element	Wavelength	E_1	E_2
	(nm)	(eV)	(eV)
Potassium	766.49	0	1.617
	769.90	0	1.610

4.4. Precision

Relative standard deviations (RSD) for the obsidian and five standard USGS basaltic glasses are shown in Fig. 5. The RSDs are the standard deviation of five sets of single-shot to 50-shot averages divided by the mean signal of the five sets of averages. For all samples, the RSDs decrease as the number of shots averaged increases. In general, the RSD values have an inverse dependence on the potassium concentration in the sample. The one exception to this trend occurs for BHVO-2G, which has a higher final RSD than BIR-1G. The RSDs for five sets of 50 shots ranged from 5.3% to 0.4% for BHVO-2G to TB-1G. It should be noted, when considering energy conservation on an in-situ extraterrestrial instrument, that little additional improvement in precision is attained above 20 laser shots.

4.5. Calibrations

To establish the effectiveness of LIBS as a tool for age dating geological materials, the measurement accuracy of potassium abundance was quantified. For these experiments, a laser pulse energy of 35 mJ, a spot size of 500 μm, and a spectrometer delay and gate of 1.5 μs and

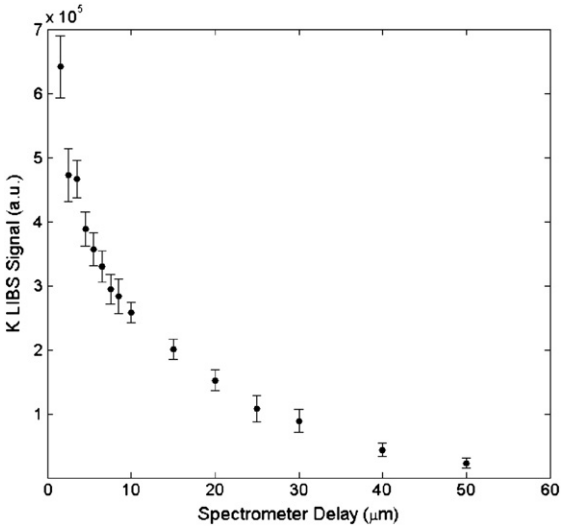

Fig. 2. Dependence of potassium signal on spectrometer delay. All data points are averages of 50 shots at one location using a spectrometer gate of 1 μs. Error bars are 1σ over the 50 shots.

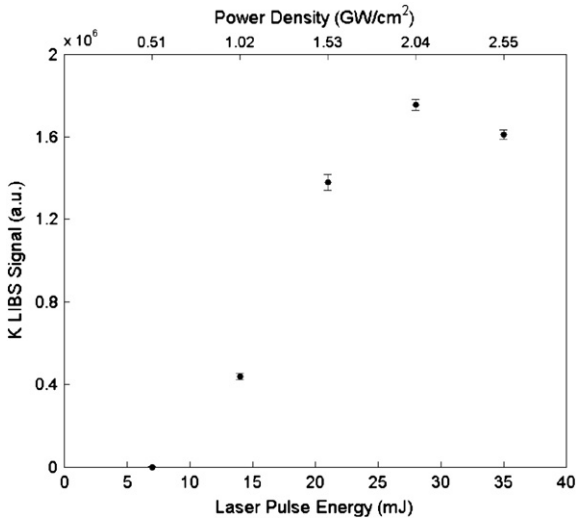

Fig. 3. Dependence of potassium signal on laser pulse energy and power density. For all measurements, the laser spot size was 500 μm and the spectrometer delay and gate were 1.5 μs and 3 μs, respectively. Error bars are 1σ over the 50 shots.

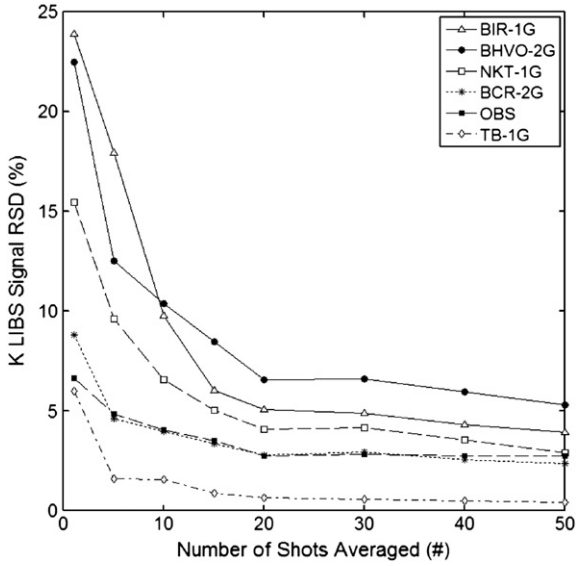

Fig. 5. Relative standard deviations (RSD) as a function of number of averaged shots for five measurements. The measurements were taken with a 500 μm laser spot, 35 mJ energy, and a 1.5 μs and 3 μs spectrometer delay and gate, respectively.

3 μs, respectively, were used. The five USGS standard samples were measured with 5 cleaning shots and 50 analytical shots at each of the 5 locations. As in the signal optimization experiments described above, the potassium signal of the USGS standards was calculated as the integrated area of the potassium doublet with baseline subtraction. For the rock samples, the signal was calculated as the integrated area of the potassium doublet normalized by the base area of the doublet. The base area of the peak consists of the area below the lower and upper wavelength limits used for the potassium peak area integration. Normalization, in this way, is expected to reduce shot-to-shot variations caused by laser energy variation and matrix effects due to the heterogeneity of the rock samples.

4.5.1. USGS standard basaltic glasses

The calibration curve of LIBS potassium signal and potassium concentration is given in Fig. 6. Potassium concentrations for the standard glasses were determined by multiple laboratories (using LA-ICP-MS, electron probe micro-analysis, ion probe, and other techniques) and compiled by the USGS [21,22]. Each LIBS data point in Fig. 6 is the average of five measurements locations, where each location was measured 50 times. The dashed lines are the boundaries of the 95% prediction bands for a non-weighted linear regression [23]. The upper electronic states of the potassium doublet undergo radiative decay to the ground state, which makes these transitions susceptible to saturation caused by self-absorption. In these experiments, measuring samples with 0.025% to 3.6% potassium by weight, the linear calibration curve suggests that self-absorption was negligible.

Predicted potassium concentrations by LIBS using non-weighted and weighted linear regressions are provided in Table 3. Each prediction is accompanied by an uncertainty range determined by the horizontal bounds of the upper and lower 95% prediction band hyperbolae. Calculations of the linear regression models and prediction bands were performed following the work by Mermet [23]. The non-weighted linear regression is the commonly applied least-squares method where a straight line is fit to the data through minimizing the sum of squares of the errors. One

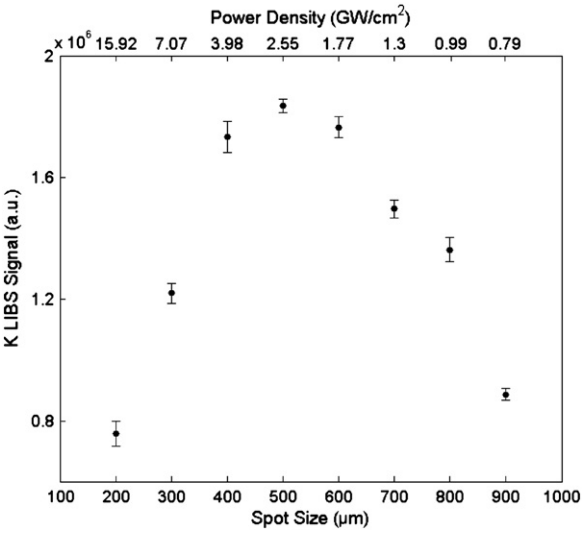

Fig. 4. Dependence of potassium signal on laser spot size and power density. All measurements are averages of 50 shots at one location at 35 mJ and a spectrometer delay and gate 1.5 μs and 3 μs, respectively. Error bars are 1σ over the 50 shots.

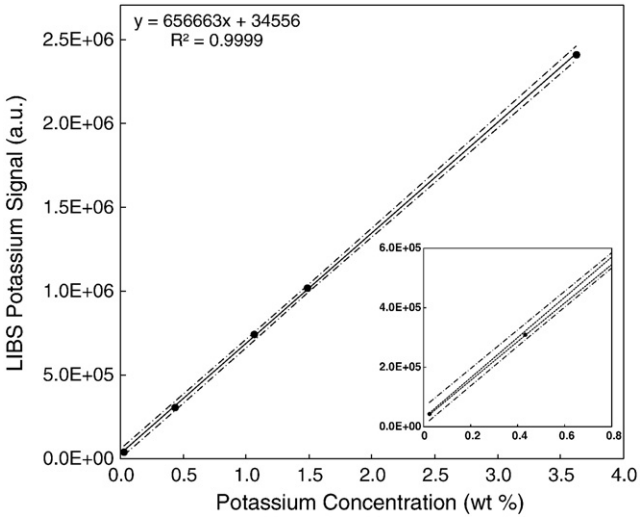

Fig. 6. Calibration of potassium signal (766.49 and 769.90 nm) and potassium concentrations for five basaltic glass standards. Each plotted point is an average of 5 replicate measurements, where each measurement is a set of 50 shots at one location. The large graph shows 95% prediction bands of the non-weighted (_._) linear regression, while the smaller inset graph shows a scaled-up view of the same data including both the non-weighted (_._) and weighted (.....) prediction bands.

Table 3
Reference and predicted potassium concentrations for basaltic glass standards using non-weighted and weighted linear regressions. Ranges are 95% prediction bands.

Sample	Reference	LIBS predictions			
		Non-weighted calibration		Weighted calibration[a]	
	(wt.%)	(wt.%)		(wt.%)	
BIR-1G	0.025	0.014	−0.046	0.025	−0.003
			+0.045		+0.003
BHVO-2G	0.432	0.420	−0.042	0.426	−0.013
			+0.041		+0.014
NKT-1G	1.062	1.081	−0.037	1.081	−0.033
			+0.037		+0.034
BCR-2G	1.486	1.502	−0.037	1.497	−0.025
			+0.037		+0.025
TB-1G	3.628	3.617	−0.059	3.589	−0.111
			+0.061		+0.115

[a] Linear regression weighed by $1/(Y^2)$, where Y = signal intensity.

important assumption made when applying the least-squares method is that the standard deviation of the difference between the measured point and the curve-fitted line, in the vertical direction, is constant over the range of concentrations measured. This is generally not the case for LIBS analysis, and it was not the case in our study. To improve predictive capabilities, especially for low concentration samples, a weighting regression procedure can be used. Here, our weighting factor was the inverse of the signal intensity squared ($1/Y^2$). This weighting factor reduces the errors for the low concentration samples at the expense of the higher concentration samples, as is shown in Table 3.

The limit of detection (LOD) and, more importantly, the limit of quantification (LOQ) provide important guidelines to constrain the sets of measureable igneous rocks that can be age dated with this technique. In lieu of the more common definitions of the LOD and LOQ ($LOD = \frac{3\cdot\sigma}{S}$ and $LOQ = \frac{10\cdot\sigma}{S}$) [24], an alternative approach will be used [25]. The LOD is found by drawing a horizontal line from the upper prediction band y-intercept point to the calibration curve. The corresponding concentration at the point on the calibration curve is the lowest concentration that can be predicted above zero 95% of the time. The LOQ is then found as the corresponding concentration where this horizontal line intersects the lower prediction band. Following this approach and using the non-weighted calibration, the LOD and LOQ for the standard glasses are 471 and 920 ppm, respectively. For the weighted calibration, the LOD and LOQ are 35 and 66 ppm, respectively.

4.5.2. Basaltic rocks

Of the five standard glass samples, four equivalent rocks in their natural form where acquired and measured (BIR-1, BHVO-2, NKT-1, and BCR-2). A rock sample of TB-1 was not located for testing. In an effort to capture the heterogeneous nature of the rock samples, 25 locations were measured on each sample with 5 cleaning and 50 analytical shots. Recent work by Anderson et al. shows that to achieve a measurement result within one standard deviation of the actual bulk composition requires measurements at 10 to 20 locations for fine and coarse grained rocks, respectively [26].

The rock samples, in our study, showed larger potassium signal variation than the standard glass samples, likely due to variations in the optical and material properties of the heterogeneous rocks. To normalize the shot-to-shot variations in the material removal, plasma formation, and resulting atomic emission, the area integrated potassium doublet was divided by the base area of the peak (P/B) [9].

Fig. 7 shows the non-weighted calibration relationship between the LIBS potassium signals (P/B) and the potassium concentrations and the corresponding 95% prediction bands. Each data point is the average signal measured across 25 locations. Table 4 shows the LIBS predicted concentrations using the non-weighted and weighted calibration approaches. For the non-weighted model, the LOD and LOQ are

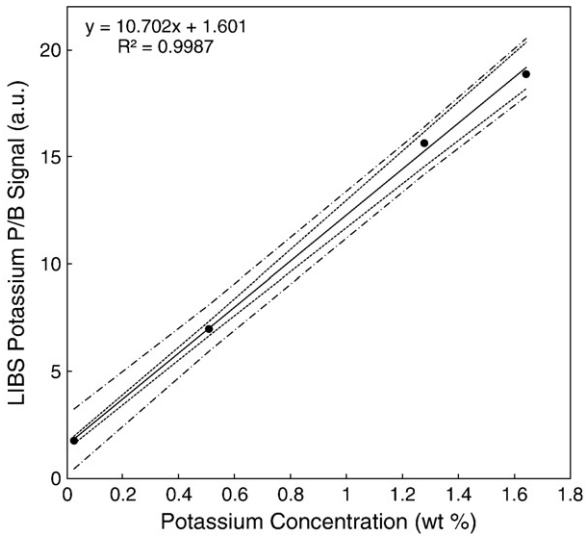

Fig. 7. Calibration of potassium peak/base signal and potassium concentrations for four basaltic rock samples. Each plotted point is an average of 5 replicate measurements, where each measurement is a set of 50 shots at one location. Dashed lines are 95% prediction bands of the non-weighted linear regression.

0.151% and 0.265% by weight, respectively. For the weighted calibration, the LOD and LOQ are 169 and 328 ppm, respectively.

4.6. Age dating by LIBS

To fully quantify the error in age determination, errors from the LIBS measurements of potassium, the mass spectrometer measurements of ^{40}Ar, and the contribution and correction scheme for excess ^{40}Ar must be considered. Here, we only estimate the error in age prediction as a result of LIBS inaccuracies. A more complete performance evaluation will be conducted in the future once both instruments are operational.

A summary of the estimated errors in age determination is given in Table 5 for both the glass standards and the basaltic rocks using the non-weighted and weighted calibration methods. Errors are estimated assuming samples ages ranging from 3000 Ma to 100 Ma. To estimate the errors, the ^{40}Ar concentration is calculated using Eq. (3) by inputting the reference (e.g., known) concentration of potassium for each sample and an assumed age. This calculation is performed separately on all samples in the glass and rock sets. Next, a linear regression of a plot of measured potassium concentrations and calculated ^{40}Ar concentrations is used to determine the slope of the isochron. A 95% confidence interval on the slope is found using the standard error in the slope and the critical *t* value.

For the glass standards, the estimated age errors range from approximately ±30 Ma for 3000 Ma samples to ±2 Ma for 100 Ma samples.

Table 4
Reference and predicted potassium concentrations for basaltic rocks using non-weighted and weighted linear regressions. Ranges are 95% prediction bands.

Sample	Reference	LIBS predictions			
		Non-weighted calibration		Weighted calibration[a]	
	(wt.%)	(wt.%)		(wt.%)	
BIR-1	0.025	0.018	−0.142	0.025	−0.016
			+0.122		+0.016
BHVO-2	0.508	0.506	−0.106	0.508	−0.038
			+0.097		+0.041
NKT-1	1.278	1.314	−0.099	1.309	−0.090
			+0.109		+0.100
BCR-2	1.642	1.615	−0.118	1.607	−0.115
			+0.136		+0.128

[a] Linear regression weighed by $1/(Y^2)$, where *Y* = signal intensity.

Table 5
Errors in age determination of the standard glasses and rock samples by LIBS.

Age	Age error range, standard glasses		Age error range, rocks	
	Non-weighted LIBS calibration	Weighted LIBS calibration	Non-weighted LIBS calibration	Weighted LIBS calibration
(Ma)	(Ma)	(Ma)	(Ma)	(Ma)
3000	−29.3	−30.0	−112.8	−113.9
	+30.1	+30.8	+124.2	+124.9
1000	−15.4	−15.8	−58.4	−58.9
	+15.9	+16.3	+66.3	+66.9
500	−8.7	−9.0	−33.0	−33.3
	+9.0	+9.3	+38.0	+38.4
100	−1.9	−2.0	−7.3	−7.4
	+2.0	+2.1	+8.5	+8.6

Earlier, we showed that the weighted calibration improves the accuracy of predicted potassium concentration, especially for the lowest concentrated sample, BIR-1G. Yet, here, there is no measurable improvement in the age errors because a small absolute change in the predicted potassium concentration for BIR-1 G has little effect on the isochron slope. For the basaltic rocks, the age errors range from approximately ± 120 Ma for 3000 Ma samples and ± 8 Ma for 100 Ma samples. These uncertainties are acceptable for improving the current understanding of Martian geological history; however, it is clear that higher errors are expected once inaccuracies in mass spectrometer readings, uncertainties of excess ^{40}Ar, and generally poorer performance of flight-ready instrumentation components are included.

5. Conclusions

The efficacy of LIBS as a method for quantifying potassium concentrations in standard basaltic glasses and basaltic rock samples was explored to assess the potential of an in-situ geochronology instrument for Mars. These initial results suggest that LIBS is capable of quantifying potassium concentration with sufficient precision, accuracy, and dynamic range to drastically improve current Martian surface ages. Using Bogard's recent numerical modeling work on simulated K–Ar isochrons under assumed instrumentation precisions for potassium measurements, the expected usefulness of our instrument can be placed in context [27]. Bogard states that, "to achieve K–Ar isochron ages on Mars to a reliability of a few tens of percent, a suite of approximately 10 samples must vary in total K concentration by a factor of two or greater, if analytical measurement precision of K and Ar are ± 10%." In our study, we accurately quantified samples that vary in potassium concentration by over a factor of eight with instrumentation precisions from 0.4 to 5.3%, meeting Bogard's criteria. Current age-dating uncertainties associated with crater counting are estimated to be roughly a factor of 2 to 4 [5]. Considering only errors in potassium measurements by LIBS, estimated age errors for the glasses range from approximately ± 30 Ma for 3000 Ma samples to ± 2 Ma for 100 Ma samples. For the basaltic rocks, the age errors are approximately ± 120 Ma for 3000 Ma samples and ± 8 Ma for 100 Ma samples. Future studies will focus on determining the error associated with argon measurements by mass spectrometry and developing a LIBS measurement system using "flight ready" system components that can handle the harsh Marian environment. In addition, a much larger set of samples having a larger variation of chemical matrix will be studied, which may require exploring multivariate data analysis approaches to account for matrix effects.

Acknowledgements

The authors would like to thank Niels Oskarsson of the Institute of Geosciences at the University of Iceland for sharing the BIR-1 rock sample, Steve Wilson of the U.S.G.S. for the BCR-2 and NKT-1 samples, and Photon Machines, Inc. for the use of their equipment and for thoughtful discussions. This work was funded by the Keck Institute for Space Studies (Award# 9900600 to Caltech), the Seattle University Faculty Sabbatical Program, and the Welch Fund for Undergraduate Research.

References

[1] K.L. Tanaka, The Stratigraphy of Mars, Proceedings of the 17th Lunar and Planetary Science Conference, Part 1, J. Geophys. Res. 91 (1986) E129–E158.
[2] D. Stoffler, G. Ryder, Stratigraphy and isotope ages of lunar geologic units: chronological standard for the inner solar system, Space Sci. Rev. 96 (2001) 9–54.
[3] G. Neukum, B.A. Ivanov, W.K. Hartmann, Cratering records in the inner solar system in relation to the lunar reference system, Chronol. Evol. Mars 96 (2001) 55–86.
[4] G.G. Michael, G. Neukum, Planetary surface dating from crater size-frequency distribution measurements: partial resurfacing events and statistical age uncertainty, Earth Planet. Sci. Lett. 294 (2010) 223–229.
[5] W.K. Hartmann, Martian cratering VI: crater count isochrons and evidence for recent volcanism from Mars global surveyor, Meteorit. Planet. Sci. 34 (1999) 167–177.
[6] W.K. Hartmann, G. Neukum, Cratering chronology and the evolution of Mars, Space Sci. Rev. 96 (2001) 165–194.
[7] L.E. Nyquist, D.D. Bogard, C.-Y. Shih, A. Greshake, D. Stoffler, O. Eugster, Ages and geologic histories of Martian meteorites, Chronol. Evol. Mars 96 (2001) 105–164.
[8] S. Kelley, K–Ar and Ar–Ar Dating, Rev. Mineral. Geochem. 47 (2002) 785–818.
[9] D.A. Cremers, L.J. Radziemski, Handbook of Laser-Induced Breakdown Spectroscopy, John Wiley & Sons, West Sussex, England, 2006.
[10] B. Salle, D.A. Cremers, S. Maurice, R.C. Wiens, P. Fichet, Evaluation of a compact spectrograph for in-situ and stand-off laser-induced breakdown spectroscopy analyses of geological samples on Mars missions, Spectrochim. Acta Part B 60 (2005) 805–815.
[11] S.M. Clegg, E. Sklute, M. Darby Dyar, J.E. Barefield, R.C. Wiens, Multivariate analysis of remote laser-induced breakdown spectroscopy spectra using partial least squares, principal component analysis, and related techniques, Spectrochim. Acta Part B 64 (2009) 79–88.
[12] A.K. Knight, N.L. Scherbarth, D.A. Cremers, M.J. Ferris, Characterization of Laser-Induced Breakdown Spectroscopy (LIBS) for application to space exploration, Appl. Spectrosc. 54 (2000) 331–340.
[13] R.C. Wiens, S. Maurice, S. Bender, B.L. Barraclough, A. Cousin, O. Forni, A. Ollila, H. Newsom, D. Vaniman, S.M. Clegg, J.A. Lasue, D. Blaney, L. DeFlores, R.V. Morris, Calibration of the MSL/ChemCam/LIBS Remote Sensing Composition Instrument, Lunar and Planetary Science Conference, XLII, 2370, The Woodlands, TX, 2011, p. 2.
[14] M. Dell'Aglio, A. De Giacomo, R. Gaudiuso, O. De Pascale, G.S. Senesi, S. Longo, Laser induced breakdown spectroscopy applications to meteorites: chemical analysis and composition profiles, Geochim. Cosmochim. Acta 74 (2010) 7329–7339.
[15] J.R. Thompson, R.C. Wiens, J.E. Barefield, D. Vaniman, H. Newsom, S.M. Clegg, Remote laser-induced breakdown spectroscopy analyses of Dar al Gani 476 and Zagami Martian meteorites, J. Geophys. Res. 111 (2005) 1–9.
[16] F. Colao, R. Fantoni, V. Lazic, A. Paolini, F. Fabbri, G.G. Ori, L. Marinangeli, A. Baliva, Investigation of LIBS feasibility for in-situ planetary exploration: an analysis on Martian rock analogues, Planet. Space Sci. 52 (2004) 117–123.
[17] T.D. Swindle, R. Bode, W.V. Boynton, D.A. Kring, M. Williams, A. Chutjian, M.R. Darrach, D.A. Cremers, R.C. Wiens, S.L. Baldwin, AGE (Argon Geochronology Experiment): an instrument for in situ geochronology on the surface of Mars, LPS XXXIV, Abstract 1488, 2003, pp. 1–2.
[18] J. Sole, In situ K/Ar geochronology using simultaneous LIBS and noble gas mass spectrometry, Goldschmidt Conference, Vancourver, Canada, 2008, p. A881.
[19] C.B. Stipe, B.D. Hensley, J.L. Boersema, S.G. Buckley, Laser-induced breakdown spectroscopy of steel: a comparison of univariate and multivariate calibration methods, Appl. Spectrosc. 64 (2010) 154–160.
[20] F. Colao, R. Fantoni, V. Lazic, A. Paolini, LIBS application for analyses of Martian crust analogues: search for the optimal experimental parameters in air and CO_2 atmosphere, Appl. Phys. A 79 (2004) 143–152.
[21] S.A. Wilson, P.A. Potts, Development of microanalytical reference materials for geochemical analysis, Microsc. Microanal. 10 (2004) 928–929.
[22] P.A. Potts, M. Thompson, S.A. Wilson, G-Probe-1—an international proficiency test for microprobe laboratories—report on round 1: February 2002 (TB-1 Basaltic Glass), Geostand. Newslett. 26 (2002) 197–235.
[23] J.M. Mermet, Calibration in atomic spectrometry: a tutorial review dealing with quality criteria, weighting procedures and possible curvatures, Spectrochim. Acta Part B 65 (2010) 509–523.
[24] IUPAC, Compendium of Chemical Terminology, 2nd ed. IUPAC, Research Triangle Park, NC, 1997.
[25] J.M. Mermet, Limit of quantitation in atomic spectrometry: an unambiguous concept? Spectrochim. Acta Part B 63 (2008) 166–182.
[26] R.B. Anderson, R.V. Morris, S.M. Clegg, J.F. Bell III, R.C. Wiens, S.D. Humphries, S.A. Mertzman, T.G. Graff, R. McInroy, The influence of multivariate analysis methods and target grain size on the accuracy of remote quantitative chemical analysis of rocks using laser induced breakdown spectroscopy, Icarus 215 (2011) 608–627.
[27] D.D. Bogard, K–Ar Dating of rocks on Mars: requirements from Martian meteorite analyses and isochron modeling, Meteorit. Planet. Sci. 44 (2009) 3–14.